

Nanoscale Coating of LiMO_2 ($M = \text{Ni, Co, Mn}$) Nanobelts with Li^+ -Conductive Li_2TiO_3 : Toward Better Rate Capabilities for Li-Ion Batteries

Jun Lu, Qing Peng,* Weiyang Wang, Caiyun Nan, Lihong Li, and Yadong Li

Department of Chemistry, State Key Laboratory of Low-Dimensional Quantum Physics, Tsinghua University, Beijing 100084

S Supporting Information

ABSTRACT: By using a novel coating approach based on the reaction between $\text{MC}_2\text{O}_4 \cdot x\text{H}_2\text{O}$ and $\text{Ti}(\text{OC}_4\text{H}_9)_4$, a series of nanoscale Li_2TiO_3 -coated LiMO_2 nanobelts with varied Ni, Co, and Mn contents was prepared for the first time. The complete, thin Li_2TiO_3 coating layer strongly adheres to the host material and has a 3D diffusion path for Li^+ ions. It is doped with Ni^{2+} and Co^{3+} ions in addition to Ti^{4+} in LiMO_2 , both of which were found to favor Li^+ -ion transfer at the interface. As a result, the coated nanobelts show improved rate, cycling, and thermal capabilities when used as the cathode for Li-ion battery.

To meet more demanding requirements for storage and utilization of clean energy, Li-ion batteries have been urged for lower cost, faster charging/discharging rate, higher capacity, longer cycling life, and better environmental benignancy.^{1–6} Layered lithium-mixed transition metal oxides, LiMO_2 ($M = \text{Ni, Co, Mn}$) have been regarded as prospective alternatives for LiCoO_2 toward better Li-ion batteries, due to their unique properties including high energy density, good cycling stability, low cost, and low toxicity.^{7–12} Nevertheless, there remain challenges for LiMO_2 materials. First, the intrinsic low Li^+ -ion conductivity of LiMO_2 prevents the improvement of high rate capability. Second, the instability of de-lithiated phase of LiMO_2 in organic electrolyte causes safety issues and capacity fading due to the high reactivity of Co^{4+} and Ni^{4+} . Coating with electrochemically inert oxides and phosphates has been an important and efficient approach to enhance the electrochemical performances of LiMO_2 .^{13–17} However, coating materials are generally unfavorable for both Li^+ -ion conduction of cathode materials and interfacial charge transfer of the electrode, not only because they behave as insulators for Li^+ -ion conduction, but also because they increase Li^+ -diffusion length resulting in deterioration of electrochemical performance.¹⁸

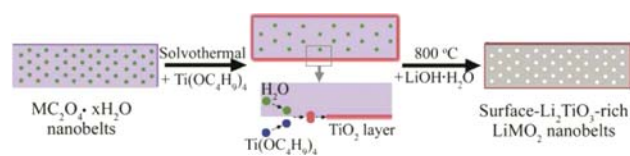
Monoclinic Li_2TiO_3 , a layered material similar to Li_2MnO_3 , has the interlamellar (002) d -spacing value of 0.480 nm which matches well with (003) d -spacing of LiMO_2 (0.468 nm). Li_2TiO_3 is electrochemically inert in a wide voltage range with excellent structural stability in organic electrolyte.^{19,20} More importantly, Li_2TiO_3 has a three-dimensional path for Li^+ -ion diffusion, in which Li^+ -ion migration can take place in (003) plane and along c direction.²¹ It has been reported that the ionic conductivity of Li_2TiO_3 would increase when doped with aliovalent ions.^{22,23} In this regard, it is possible that a thin,

complete and doped Li_2TiO_3 coating layer can help to improve the rate capability as well as the cycling stability of LiMO_2 materials, which will be significant to the performance improvement of various cathode materials.^{24–26}

As to the coating route, traditional approaches such as mechanical mixing, sol–gel, and atomic deposition methods have been developed.^{27–29} However, these methods cannot establish a uniform, complete, robust and controllable coating layer on the host materials. Specifically, with mechanical method it is difficult to build a complete coating layer on the host materials, because the coating particles distribute randomly on the surface of the host materials. For sol–gel method, the thickness of the coating layer is difficult to be uniform due to a similar reason. Finally, for all these methods the coating layers are formed by post-coating routes under a relatively low temperature, resulting in the weak bonding between the host and the coating layer.

Toward better surface-modified cathode materials, we prepared a series of surface- Li_2TiO_3 -rich LiMO_2 ($M = \text{Ni, Co, and Mn}$) nanobelts (Ni:Co:Mn = 8:1:1, 6:2:2 and 4:3:3 in molar ratio) with Ti:(Ni+Co+Mn) = 5:100 in molar ratio. We used a novel and general coating approach, in which a robust, uniform, and complete nanoscale Li_2TiO_3 layer doped with Co^{3+} and Ni^{2+} ions has been achieved. The synthetic approach of the nanobelts consists of two steps, in which TiO_2 -coated $\text{MC}_2\text{O}_4 \cdot x\text{H}_2\text{O}$ nanobelts were prepared first, and then the nanobelts were lithiated to give the coated product (Scheme 1).

Scheme 1. Two-Step Approach for Surface Li_2TiO_3 -Rich LiMO_2 Nanobelts



Mixed metal oxalate nanobelts were chosen as the precursors, not only due to their 1D nanobelt structures, but also because their dehydration reaction can occur at around $150\text{ }^\circ\text{C}$ (see TGA curves in Figure SI 1a). The uniform TiO_2 coating of $\text{MC}_2\text{O}_4 \cdot x\text{H}_2\text{O}$ nanobelts was based on a smart approach, in which highly reactive $\text{Ti}(\text{OC}_4\text{H}_9)_4$ reacts with H_2O molecules released by the nanobelts at $150\text{ }^\circ\text{C}$ under solvothermal

Received: September 2, 2012

Published: January 9, 2013

condition, forming a uniform coating layer on the surface of the nanobelts. The products (denoted as Ti811, Ti622, and Ti433) obtained from calcination at 800 °C (the optimized temperature range for layered oxides) match with identical α - NaFeO_2 layered structure with clear (006) and (012) peaks around 38° (Figure 1a).³⁰ It should be noted that no peaks corresponding

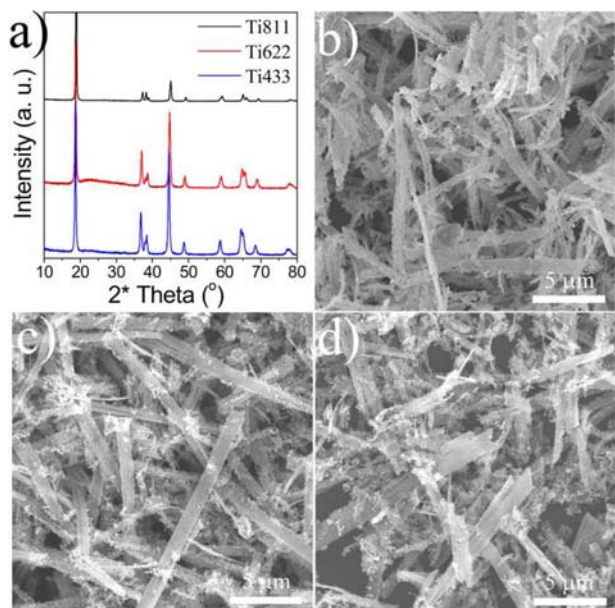


Figure 1. (a) XRD pattern of a series of coated LiMO_2 products. (b–d) SEM images of Ti811 (b), Ti622 (c), and Ti433 (d) nanobelts.

to monoclinic Li_2TiO_3 could be found, presumably due to the low loading content and the formation of layered $\text{Li}[\text{Ni}_x\text{Co}_y\text{Ti}_z]\text{O}_2$ domains in the surface layer of Li_2TiO_3 .³¹ By increasing the Ti:(Ni+Co+Mn) content to 15:100 for Ti433 nanobelts, characteristic peaks for monoclinic Li_2TiO_3 around 20.82° began to appear (Figure SI 2). This may demonstrate that Li_2TiO_3 was formed during the calcination with stoichiometric Li salt, though it was not detectable with Li_2TiO_3 -coated samples with Ti:(Ni+Co+Mn) = 5:100 by XRD. Also, it should be noted that Ti^{4+} ions enter into the layered structure as doping ions, which is indicated by the increase of lattice parameters for coated materials (Table SI 1).

The prepared Ti811, Ti622, and Ti433 materials show the 1D nanobelt structure under SEM in Figure 1b–d. It is remarkable that the 1D morphologies for all coated and pristine materials have survived through the calcination at 800 °C (Figure SI 3). The nanobelts composed of about 100 nm primary nanograins are approximately 15 μm in length, 1.5 μm in width, and 100 nm in thickness, with a length/thickness ratio of 100. The one-dimensional nanostructure, and porous structures due to the considerable weight loss during calcination, would both benefit the rate performance.^{32,33} Also, the coated nanobelts show negligible improvement in specific surface area over the pristine materials. Taking the Ti433 and pristine 433 samples as the example, the BET surface areas are 6.22 and 5.89 m^2g^{-1} respectively, with about 5% difference.

For further characterization, Ti433 nanobelts were selected as the representative for the three nanobelts. The polycrystalline Ti433 nanobelt is composed of nanograins under high-resolution transmission electron microscopy (HRTEM)

(Figure 2a). In selected-area electron diffraction (SAED) in Figure 2b, the bright diffraction spot with a 0.47 nm d -spacing

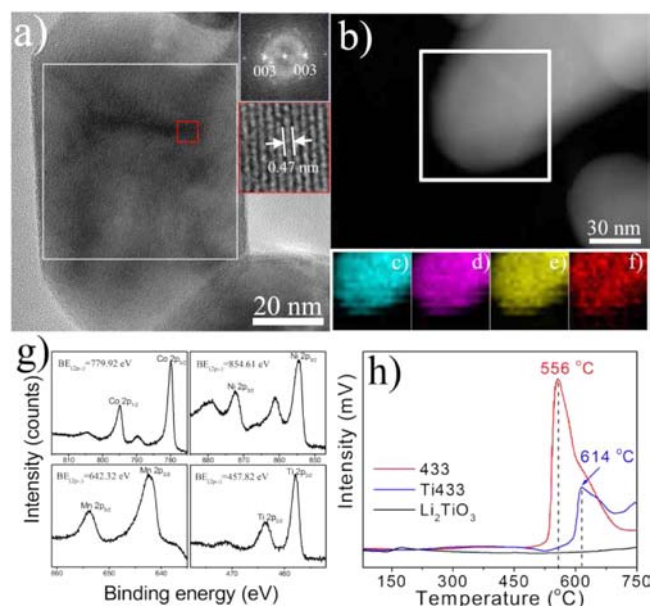


Figure 2. (a) HRTEM images of Ti433 nanobelts; insets show SAED and lattice fringes. (b) High-angle annular dark-field scanning TEM (HAADF-STEM) of T433 sample. (c–f) Elemental mapping results of Co (c), Ni (d), Mn (e), and Ti (f). (g) XPS spectra for Co, Ni, Mn, and Ti elements of Ti433 nanobelts. (h) CO-TPR profiles for coated LiMO_2 , pristine, and reference Li_2TiO_3 .

is ascribed to the (003) facet of LiMO_2 . Elemental mapping for Ti, Mn, Co, and Ni in Figure 2c–f shows that the elements uniformly distribute in the selected region of the Ti433 nanograin, indicating that the obtained materials were uniformly coated.

To address the Li_2TiO_3 coating layer, surface-sensitive characterizations have been applied. In a similar case, the complexity of structure of the $(1-x)\text{LiMO}_2 \cdot x\text{Li}_2\text{MnO}_3$ has been investigated via convergent beam electron diffraction and Li^7 MAS NMR.²⁸ However, these methods are not appropriate for the characterization of the coating layer on nanostructures. Instead, X-ray photoelectron spectroscopy (XPS) has been used to determine the surface content of elements (Figure 2g), because only photoelectrons from atoms neighboring to the interface within 8–10 nm are collected by XPS.³⁴ By XPS characterization, the valences are determined to be 3+, 2+, 4+, and 4+ for Co, Ni, Mn, and Ti, respectively.³⁵ More importantly, the elemental quantification result of XPS indicates a Li_2TiO_3 -rich coating layer on LiMO_2 nanobelts (Table 1). Further calculations have been performed for a better understanding of the coating layer (see details below Figure SI 5). The maximum thickness is estimated to be 9 nm. Considering the loss of Ti on surface due to its penetration into the bulk, the actual thickness would be thinner. In particular,

Table 1. Atomic ratio of Ti to (Ni+Co+Mn) of Ti433 Determined from XPS and from Precursor Applied in the Synthetic Process

	XPS	starting ratio
Ti:(Ni+Co+Mn)	23:(32+46+22)	5.0:(30+40+30)

the contents of Co^{3+} and Ni^{2+} ions calculated from XPS which are higher than the bulk values indicate the doping of Co^{3+} and Ni^{2+} ions into the surface Li_2TiO_3 . As a result, the coated nanobelts are described as surface- Li_2TiO_3 -rich nanobelts, with $\text{Li}[\text{Ni}_x\text{Co}_y\text{Ti}_{1-x-y}]\text{O}_2$ domains at the surface layer.

This unique coating layer indicates a strong interaction between Li_2TiO_3 and the host structure. It brings more benefits than traditional coating layers. First, the coating-host structure is strengthened, which is essential for the long-term structural stability and cycling capability. Second, enhanced Li^+ ionic conductivity of doped Li_2TiO_3 is expected. When doped with aliovalent ions, Li^+ -ion vacancies will be increased. It reduces the repulsion of Li^+-Li^+ ions, which is in favor of fast Li^+ -ion intercalation/de-intercalation of the LiMO_2 structure.^{22,23} Therefore, enhanced rate performances of coated nanobelts are expected.

Another surface-sensitive method, carbon monoxide temperature programmed reduction (CO-TPR), was also used to address the coating uniformity of the nanobelts (Figure 2h). For Ti433 and its counterpart, the peak temperature shifted to 614 °C with low peak intensity after coating, and the original peak at 556 °C completely disappeared. The CO-TPR result indicates that a complete coating has been achieved via the synthetic approach. In addition, the reactivity of surface O^{2-} with CO has been suppressed due to the inactive Li_2TiO_3 layer, which will help to protect the di-lithiated materials from reacting with the organic electrolyte.

To determine the influence of coating layer on electrochemical performance of LiMO_2 , electrochemical tests have been carried out under 0.5–10 C (1 C = 140 mA/g) in the voltage range of 3.0–4.3 V at 25 and 55 °C (Figure 3a,b). The

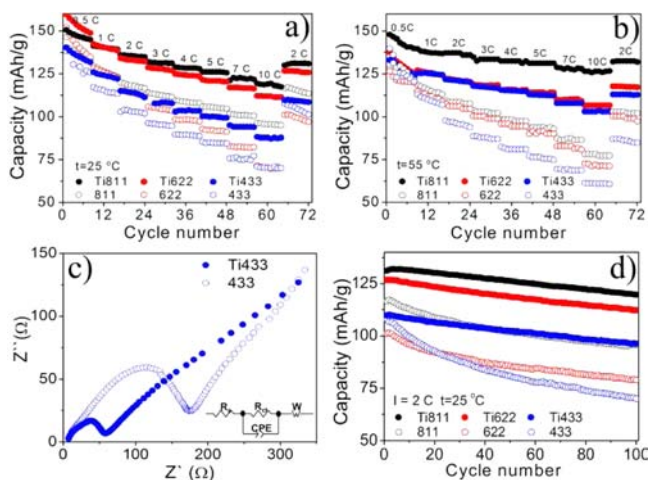


Figure 3. (a,b) Rate performance of coated and pristine LiMO_2 nanobelts under 25 (a) and 55 °C (b). (c) Nyquist plots for Ti433 and 433 nanobelts after cycling, with the equivalent circuit as the inset. (d) Capacity-cycling plots for the two series of nanobelts.

electrochemical performances of the Li_2TiO_3 coated LiMO_2 nanobelts show inspiring rate capability as well as thermal stability than the pristine counterparts. Taking Ti433 and 433 nanobelts as the example, Ti433 sample takes the capacity advantage of 25% under 10 C at 25 °C. This is compared to the 433 counterpart, which are 88 and 70 mAh/g, respectively. When the temperature is set at 55 °C, the capacity for pristine nanobelts declines mainly due to the capacity fading, while the coated material delivers larger capacity for improved Li^+ -ion

conductivity. The difference at 55 °C becomes dramatically larger, reaching 103 and 61 mAh/g, respectively. These conclusions also hold for Ti811 and Ti622 with their counterparts, with even larger differences. It should be noted that, when cycling under 55 °C, the Ti433 nanobelts exhibit a better rate performance than 811 showing the advantage of the coated materials. Furthermore, an obvious difference in resistance between the coated and pristine materials has been revealed by electrochemical impedance spectroscopy (Figure 3c). The Nyquist plots of both materials observe the same equivalent circuit. In particular, the charge transfer resistances for the coated LiMO_2 are much smaller than those for the uncoated materials (Table SI 2). This observation indicates that Li_2TiO_3 layer effectively reduces the barrier for Li^+ -ion transfer at the electrode–electrolyte interface. The outstanding rate performance as well as the reduced charge transfer resistance of coated nanobelts is attributed to the unique coating layer of the nanobelts, the three-dimensional path for Li^+ -ion migration and the aliovalent ion doped structure of Li_2TiO_3 . These features improve the velocity of interfacial Li^+ -transfer processes, enhancing the rate capability of the coated nanobelts.

Coated nanobelts also exhibit better capacity retention than the pristine nanobelts when cycling at 2 C (Figure 3d, Table SI 4). This is ascribed to the suppression of side reactions with the electrolyte, which protects the LiMO_2 materials from dissolution into the electrolyte. In addition, doping of Ti^{4+} also helps to improve the structural stability, while the effect on the rate enhancement is limited as the differences in Li^+ -ion diffusion coefficients for coated and uncoated samples are minor (Table SI 3). Due to this reason, the Li_2TiO_3 -coated nanobelts could be capable for cycling under higher cutoff voltage, which will increase the capacity that material deliver.

In conclusion, a series of 1D surface- Li_2TiO_3 -rich LiMO_2 ($M = \text{Ni}, \text{Co}, \text{and Mn}$) nanobelts have been prepared by a smart and versatile coating approach. The prepared nanobelts exhibit impressive rate capability benefiting from the coating layer. The Li_2TiO_3 -rich surface layer has been demonstrated via XPS and CO-TPR methods. It is found that (1) Li_2TiO_3 -rich layer covers the surface layer completely; (2) it is well diluted by the LiMO_2 host structure, which strengthens the bonding between the coating layer and host material; (3) Li_2TiO_3 is doped by Ni^{2+} and Co^{3+} ions, which will benefit the ionic conductivity; and (4) the coating layer stabilizes host LiMO_2 structure from CO reduction, which indicates the suppression of coated materials to the electrochemical side reactions at high voltage. Finally, impressive rate performances as well as cycling and thermal stability have been demonstrated for Li_2TiO_3 -rich LiMO_2 nanobelts, due to the Li_2TiO_3 -rich surface. The inert and uniform Li_2TiO_3 -rich surface doped with Ni^{2+} and Co^{3+} , and the 3D path for Li^+ -ion diffusion, are proposed as the reasons for the inspiring enhancement of electrochemical performances.

■ ASSOCIATED CONTENT

📄 Supporting Information

Detailed experimental procedures and characterization methods; TGA curve for the $\text{MC}_2\text{O}_4 \cdot x\text{H}_2\text{O}$ nanobelts; HRTEM image for TiO_2 coated MC_2O_4 (Ti433); retrieved crystal lattice parameters for coated and uncoated materials; XRD pattern of 433 nanobelts with Ti:M ratio of 15:100; XRD patterns and SEM images for 811, 622, and 433 nanobelts; EDS of Ti433; XPS and quantity analysis of surface Ti for Ti433 sample; fitting details for Nyquist plots of Ti433 and its pristine

counterpart. This material is available free of charge via the Internet at <http://pubs.acs.org>.

AUTHOR INFORMATION

Corresponding Author

pengqing@mail.tsinghua.edu.cn

Notes

The authors declare no competing financial interest.

ACKNOWLEDGMENTS

This work was supported by the State Key Project of Fundamental Research for Nanoscience and Nanotechnology (2011CB932401, 2011CBA00500) and NSFC (20921001, 21171105, 21231005). We are grateful for Vice Professor Jiaping Wang and experimental assistant Fei Zhao in Tsinghua-Foxconn Nanocenter for their generous help on the assembly of batteries.

REFERENCES

- (1) Tarascon, J. M.; Armand, M. *Nature* **2001**, *414*, 359.
- (2) Guo, Y. G.; Hu, J. S.; Wan, L. J. *Adv. Mater.* **2008**, *20*, 2878.
- (3) Manthiram, A.; Murugan, A. V.; Sarkar, A.; Muraliganth, T. *Energ. Environ. Sci.* **2008**, *1*, 621.
- (4) Chen, J.; Cheng, F. Y. *Acc. Chem. Res.* **2009**, *42*, 713.
- (5) Li, H.; Wang, Z. X.; Chen, L. Q.; Huang, X. J. *Adv. Mater.* **2009**, *21*, 4593.
- (6) Goodenough, J. B.; Kim, Y. *Chem. Mater.* **2010**, *22*, 587.
- (7) Liu, Z.; Yu, A.; Lee, J. Y. *J. Power Sources* **1999**, *81–82*, 416.
- (8) Ohzuku, T.; Makimura, Y. *Chem. Lett.* **2001**, *30*, 642.
- (9) Kim, J. S.; Johnson, C. S.; Thackeray, M. M. *Electrochem. Commun.* **2002**, *4*, 205.
- (10) Whittingham, M. S. *Chem. Rev.* **2004**, *104*, 4271.
- (11) Thackeray, M. M.; Kang, S. H.; Johnson, C. S.; Vaughey, J. T.; Benedek, R.; Hackney, S. A. *J. Mater. Chem.* **2007**, *17*, 3112.
- (12) Bruce, P. G.; Scrosati, B.; Tarascon, J. M. *Angew. Chem., Int. Ed.* **2008**, *47*, 2930.
- (13) Cho, J.; Kim, Y. J.; Kim, T. J.; Park, B. *Angew. Chem., Int. Ed.* **2001**, *40*, 3367.
- (14) Cho, J.; Kim, Y.-W.; Kim, B.; Lee, J.-G.; Park, B. *Angew. Chem., Int. Ed.* **2003**, *42*, 1618.
- (15) Thackeray, M. M.; Johnson, C. S.; Kim, J. S.; Lauzze, K. C.; Vaughey, J. T.; Dietz, N.; Abraham, D.; Hackney, S. A.; Zeltner, W.; Anderson, M. A. *Electrochem. Commun.* **2003**, *5*, 752.
- (16) Li, C.; Zhang, H. P.; Fu, L. J.; Liu, H.; Wu, Y. P.; Rahm, E.; Holze, R.; Wu, H. Q. *Electrochim. Acta* **2006**, *51*, 3872.
- (17) Lim, S.; Cho, J. *Chem. Commun.* **2008**, 4472.
- (18) Park, J.-H.; Cho, J.-H.; Kim, S.-B.; Kim, W.-S.; Lee, S.-Y.; Lee, S.-Y. *J. Mater. Chem.* **2012**, *22*, 12574.
- (19) Dorrian, J. F.; Newnham, R. E. *Mater. Res. Bull.* **1969**, *4*, 179.
- (20) Kannan, A. M.; Rabenberg, L.; Manthiram, A. *Electrochem. Solid State Lett.* **2003**, *6*, A16.
- (21) Vijayakumar, M.; Kerisit, S.; Yang, Z. G.; Graff, G. L.; Liu, J.; Sears, J. A.; Burton, S. D.; Rosso, K. M.; Hu, J. Z. *J. Phys. Chem. C* **2009**, *113*, 20108.
- (22) Wu, X.; Wen, Z.; Xu, X.; Han, J. *Solid State Ionics* **2008**, *179*, 1779.
- (23) Wu, X. W.; Wen, Z. Y.; Wang, X. Y.; Xu, X. G.; Lin, J.; Song, S. F. *Fusion Eng. Des.* **2010**, *85*, 1442.
- (24) Amatucci, G. G.; Blyr, A.; Sigala, C.; Alfonse, P.; Tarascon, J. M. *Solid State Ionics* **1997**, *104*, 13.
- (25) Guo, Y. G.; Hu, Y. S.; Sigle, W.; Maier, J. *Adv. Mater.* **2007**, *19*, 2087.
- (26) Kang, B.; Ceder, G. *Nature* **2009**, *458*, 190.
- (27) Li, C.; Zhang, H. P.; Fu, L. J.; Liu, H.; Wu, Y. P.; Ram, E.; Holze, R.; Wu, H. Q. *Electrochim. Acta* **2006**, *51*, 3872.
- (28) Fu, L. J.; Liu, H.; Li, C.; Wu, Y. P.; Rahm, E.; Holze, R.; Wu, H. Q. *Solid State Sci.* **2006**, *8*, 113.
- (29) Zhao, J. P.; Wang, Y. J. *Phys. Chem. C* **2012**, *116*, 11867–1187.
- (30) Ngala, J. K.; Chernova, N. A.; Ma, M.; Mamak, M.; Zavalij, P. Y.; Whittingham, M. S. *J. Mater. Chem.* **2004**, *14*, 214.
- (31) Thackeray, M. M.; Kang, S. H.; Johnson, C. S.; Vaughey, J. T.; Hackney, S. A. *Electrochem. Commun.* **2006**, *8*, 1531.
- (32) Li, Y. G.; Tan, B.; Wu, Y. Y. *Nano Lett.* **2008**, *8*, 265.
- (33) Lee, H. W.; Muralidharan, P.; Ruffo, R.; Mari, C. M.; Cui, Y.; Kim, D. K. *Nano Lett.* **2010**, *10*, 3852.
- (34) Philippe, B.; Dedryvère, R.; Allouche, J.; Lindgren, F.; Gorgoi, M.; Rensmo, H.; Gonbeau, D.; Edström, K. *Chem. Mater.* **2012**, *24*, 1107.
- (35) Wagner, C. D.; Muilenberg, G. E. *Handbook of x-ray photoelectron spectroscopy: a reference book of standard data for use in x-ray photoelectron spectroscopy*; Perkin-Elmer Corp., Physical Electronics Division: 1979.